Experimental identification of homogenized traction and bending complex Young's modules using a local dynamic inverse method on a sandwich curved beam

Paul Bottois, Frédéric Ablitzer, Pascal Audrain, Nicolas Joly, Charles Pezerat

Version of Record: https://www.sciencedirect.com/science/article/pii/S0022460X20305162
Manuscript_394c71345fa69ac3b41ff7dbb566b988

Experimental identification of homogenized traction and bending complex Young's modules using a local dynamic inverse method on a sandwich curved beam

Paul Bottois[a,*], Frédéric Ablitzer[a], Pascal Audrain[b], Nicolas Joly[a], Charles Pézerat[a]

[a] *Laboratoire d'Acoustique de l'Université du Mans, LAUM - UMR 6613 CNRS, Le Mans Université, Avenue Olivier Messiaen, 72085 LE MANS CEDEX 9, France*
[b] *IRT Jules Verne, Chemin du Chaffault, 44340 Bouguenais, France*

Abstract

Identification of elastic and damping properties is a challenge for fabrication of composite materials, which can have complex shapes. A new approach based on the Force Analysis Technique was developed to identify structural parameters from local equation of motion. For structures with known analytical models, this method gave good results. This work presents a similar approach to extend the previous method to structures which cannot be described with known analytical models, where the model is replaced by a Finite Element operator. In order to reduce the amplification of the measurement noise, a procedure based on a probabilistic approach coupled to a minimization of a cost function is proposed. The method is illustrated on a curved beam using simulated displacement. Then, an experimental validation is shown by using measured translations on an aluminum flat beam and on a sandwich curved beam.

Keywords: inverse identification, curved beam, composite materials, complex Young's modules, Force Analysis Technique, FEM

1. Introduction

The vibro-acoustic behavior of structures made of composite materials is difficult to grasp numerically, because the modeling of each constituent may lead to a huge model, which cannot be operated. Such models can be reduced using homogenized material properties, but the assessments of homogenized properties is not straightforward. The common methods to identify structural parameters can be divided in four categories. The first category corresponds to static or quasi-static methods, which are based on the linear elastic theory of materials [1]. Although these methods are well established, they provide incomplete information, in the sense that they do not give the frequency dependence of the material properties. The second category concerns methods based on modal analysis [2, 3]. They

*Corresponding author
Email address: paul.bottois@univ-lemans.fr (Paul Bottois)

rely on the identification of natural frequencies and modal damping ratios to estimate the Young's modulus and loss factor of a material. The standardized tests [4] propose a methodology for estimating the elastic properties of multi-layer composite beams, using the Oberst beam method. The using of modal method implies a good knowledge about the boundary conditions, which is not always possible. Montalvao [5] noted a variability over the estimation of structural parameters depending on the clamping conditions. Close to these modal methods, other methods are based on the identification of the natural wavenumber of the structure, from which structural parameters can be extracted [6]. A third class of methods is based on comparison of modal parameters obtained numerically by using a Finite Element (FE) model with those obtained experimentally on the real structure. The identification of structural parameters is performed by updating the FE model until the theoretical data match the experimental data [7, 8]. The fourth family includes high frequency methods, also known as ultrasound methods [9, 10], which may be used to obtain a spatial mapping of material properties.

Following this classical methods and with the rise of full-field measurement techniques, inverse methods to identify structural parameters were developped. The Virtual Field Method (VFM) was developped at the end of 1980s by Grediac [11]. This method is based on the global equilibrium of tested sample, which can be described by the Principle of virtual work. Verifying this principle, it is also possible to identify material properties of the sample like Young's modulus or loss factor. Some works are done for the identification of the stiffness of isotropic plate [12] and of orthotropic plate [13].

At the end of 1990s, an another inverse approach was developed by Pézerat for vibration source identification [14] called Force Analysis Technique (FAT) or *Résolution Inverse Filtrée Fenêtrée* (RIFF), which stands for Windowed Filtered Inverse Resolution. This inverse method is based on the verification of the local equation of motion of a vibrating structure. It means a part of the structure can be considered without knowing what happens in others parts of the structure. The principal advantages of the proposed procedure are that it can be performed locally on the structure without the knowledge of the boundary conditions of the area of interest and any information outside this area. It can be noted that this technique is not recent and has been widely used (under different names) for the identification of sources (initially introduced in [15, 16, 17]) and location of defects (see for example [18, 19, 20]), generally in the case of analytically known structures (plate-shell beams). The identification of sources on complex structures modelled by FEM is not recent either, but its use was different since it was a question of identifying sources [21, 22]. Its adaptation to the characterization of materials on academic structures is much more recent, but it has remained limited to academic structures [18]. The basic principle of the FAT technique is to inject the discrete measured displacement field of the structure in a discrete form of its motion equation. Usually, a Finite Difference scheme is used. As the assesment of spatial derivatives of the displacement amplifies the measurement noise, the inverse problem requires a regularization step. In the FAT method, the regularization is ensured by a spatial windowing associ-

ated with a low-pass wavenumber filtering of the calculated force distribution. The main advantage of this method is that little information is required: the local equation of motion and a local displacement field. At the beginning, the method was developed only for identification of force distribution exciting the structure on analytically known structures, such as beams [15], plates [16] and shells [17].

In order to extend the FAT method and make it suitable for more complex structures, a Finite Element formulation of the inverse problem was developed by Renzi [23] for identification of source. This variant of the method gives the possibility to identify nodal loads on a finite element mesh from the measured displacements. It has been experimentally validated on flexural beams and flexural plates.

Another variant of the FAT method aims at identifying material properties (stiffness and damping) [24, 25]. It is based on the verification of the local equation of motion in an area of the structure in which no external force is applied. This approach is always independent of boundary condition and allows identification of material properties at any frequency, not only at resonant frequencies. The ability of the method to provide a spatial mapping of properties has been experimentally demonstrated by considering a composite plate containing patches of damping material [25]. Wassereau [18] extended this approach to characterize structural parameters on thick sandwich beams using Timoshenko's model. He estimated complex Young's modulus and complex shear modulus.

Since manufacturing of composite materials implies that the material and the shape of structures must be made in the same process, it is particularly interesting in characterizing composite materials on shaped parts instead of samples.

Recently, the two aforementioned variants of the FAT method have been coupled in an attempt to identify material properties on structure having complex geometries, using a FE operator. A proof-of-concept was presented considering a flat beam [26]. The estimation of a complex Young's modulus was demonstrated using numerical and experimental data. The regularization of the inverse problem was introduced by a probabilistic approach inspired from previous work by Faure [27].

In this paper, this approach is extended to the case of a curved beam, where transverse and longitudinal motions are coupled. In section 2, the general principle of the method is exposed. Then, the proposed approach is demonstrated in section 3, using a simulated displacement field. The effect of noise is illustrated and a probabilistic framework is proposed to automatically adjust the level of regularization. Finally, in section 4, the proposed approach is demonstrated on the measured translations of an aluminum flat beam and of a sandwich curved beam.

2. Identification technique

2.1. Basic principle

This part adresses the basic principle of the proposed approach. It is divided into three topics:

- building of the FE matrices,
- elimination of force at the boundary of the considered area,
- influence of the noise on the inverse problem.

Building of the FE matrices

In the following, the dynamic problem of an homogenized Euler-Bernoulli beam is considered. This beam has a thickness h, a width b, a beam section $S = hb$ and a second moment of area I_z. Its homogenized material properties are the density ρ, the traction complex Young's modulus $\tilde{E}_t = E_t(1+j\eta_t)$, where E_t is the traction Young's modulus, η_t, the traction structural damping of the material, and j the unit imaginary number and the flexural complex Young's modulus $\tilde{E_f} = E_f(1+j\eta_f)$, where E_f is the flexural Young's modulus and η_f, the flexural structural damping of the material. In this article, the beam is studied in the plane (x,z) and can have a curvature, *i.e.* its neutral axis is not straight. The curvature can be defined by a local radius that can vary along the neutral axis.

The in-plane moving beam is modeled by the Finite Element Method (FEM) with N discretizing nodes, $N_{DOF} = 3N$ degrees of freedom (DOFs) and Ne elements ($Ne = N-1$). Considering harmonic motion at angular frequency ω, the equation of motion of the discrete system can be written as [28] :

$$\left(\mathbf{K} - \omega^2\mathbf{M}\right)\mathbf{q} = \mathbf{f}, \tag{1}$$

where $\mathbf{M}$ is the mass matrix, $\mathbf{K}$ is the stiffness matrix and $\mathbf{q}$ is the response vector containing $2N$ translations and N rotations (motions in the plane) and $\mathbf{f}$ is the excitation vector containing, according to the DOFs mentioned here above, $2N$ forces and N moments.

The matrices $\mathbf{M}$ and $\mathbf{K}$ can be computed by assembling the elementary mass and stiffness matrices, $\mathbf{M^e}$ and $\mathbf{K^e}$. In the local reference frame (x,z) of each beam element (see figure 1), these matrices are defined with the FEM [28] as

$$\mathbf{M^e} = \rho S L_e \begin{bmatrix} \frac{1}{3} & 0 & 0 & \frac{1}{6} & 0 & 0 \\ 0 & \frac{13}{35} & \frac{11L_e}{210} & 0 & \frac{9}{70} & -\frac{13L_e}{420} \\ 0 & \frac{11L_e}{210} & \frac{L_e^2}{105} & 0 & \frac{13L_e}{420} & -\frac{L_e^2}{140} \\ \frac{1}{6} & 0 & 0 & \frac{1}{3} & 0 & 0 \\ 0 & \frac{9}{70} & \frac{13L_e}{420} & 0 & \frac{13}{35} & -\frac{11L_e}{210} \\ 0 & -\frac{13L_e}{420} & -\frac{L_e^2}{140} & 0 & -\frac{11L_e}{210} & \frac{L_e^2}{105} \end{bmatrix}, \tag{2}$$

and

$$\mathbf{K^e} = \begin{bmatrix} \frac{\tilde{E}_t S}{L_e} & 0 & 0 & -\frac{\tilde{E}_t S}{L_e} & 0 & 0 \\ 0 & \frac{12\tilde{E}_f I_z}{L_e^3} & \frac{6\tilde{E}_f I_z}{L_e^2} & 0 & -\frac{12\tilde{E}_f I_z}{L_e^3} & \frac{6\tilde{E}_f I_z}{L_e^2} \\ 0 & \frac{6\tilde{E}_f I_z}{L_e^2} & \frac{4\tilde{E}_f I_z}{L_e} & 0 & -\frac{6\tilde{E}_f I_z}{L_e^2} & \frac{2\tilde{E}_f I_z}{L_e} \\ -\frac{\tilde{E}_t S}{L_e} & 0 & 0 & \frac{\tilde{E}_t S}{L_e} & 0 & 0 \\ 0 & -\frac{12\tilde{E}_f I_z}{L_e^3} & -\frac{6\tilde{E}_f I_z}{L_e^2} & 0 & \frac{12\tilde{E}_f I_z}{L_e^3} & -\frac{6\tilde{E}_f I_z}{L_e^2} \\ 0 & \frac{6\tilde{E}_f I_z}{L_e^2} & \frac{2\tilde{E}_f I_z}{L_e} & 0 & -\frac{6\tilde{E}_f I_z}{L_e^2} & \frac{4\tilde{E}_f I_z}{L_e} \end{bmatrix}, \tag{3}$$

where L_e is the length of the beam element.

The stiffness elementary matrix (Eq. (3)) can be rewritten as

$$\mathbf{K^e} = \tilde{E}_t \mathbf{K_t^e} + \tilde{E}_f \mathbf{K_f^e}, \tag{4}$$

where

$$\mathbf{K_t^e} = \begin{bmatrix} \frac{S}{L_e} & 0 & 0 & -\frac{S}{L_e} & 0 & 0 \\ 0 & 0 & 0 & 0 & 0 & 0 \\ 0 & 0 & 0 & 0 & 0 & 0 \\ -\frac{S}{L_e} & 0 & 0 & \frac{S}{L_e} & 0 & 0 \\ 0 & 0 & 0 & 0 & 0 & 0 \\ 0 & 0 & 0 & 0 & 0 & 0 \end{bmatrix} \tag{5}$$

is the matrix providing the geometric contribution to the traction stiffness matrix of the element and

$$\mathbf{K_f^e} = \begin{bmatrix} 0 & 0 & 0 & 0 & 0 & 0 \\ 0 & \frac{12I_z}{L_e^3} & \frac{6I_z}{L_e^2} & 0 & -\frac{12I_z}{L_e^3} & \frac{6I_z}{L_e^2} \\ 0 & \frac{6I_z}{L_e^2} & \frac{4I_z}{L_e} & 0 & -\frac{6I_z}{L_e^2} & \frac{2I_z}{L_e} \\ 0 & 0 & 0 & 0 & 0 & 0 \\ 0 & -\frac{12I_z}{L_e^3} & -\frac{6I_z}{L_e^2} & 0 & \frac{12I_z}{L_e^3} & -\frac{6I_z}{L_e^2} \\ 0 & \frac{6I_z}{L_e^2} & \frac{2I_z}{L_e} & 0 & -\frac{6I_z}{L_e^2} & \frac{4I_z}{L_e} \end{bmatrix} \tag{6}$$

is the matrix providing the geometric contribution to the bending stiffness matrix of the element.

Both matrices are formulated in terms of local coordinates, *i.e.* with respect to local axes (x,z) shown in figure 1. To obtain the assembled mass matrix $\mathbf{M}$ and the assembled stiffness matrices $\mathbf{K_t}$ and $\mathbf{K_f}$, the elementary matrices have to be expressed with respect to the global axes (X_S,Z_S), also called structural axes, see figure 1. Geradin [28] proposes a transformation matrix $\mathbf{T^e}$ which allows to compute the elementary mass and stiffness matrices of each element with respect to global axes as

$$\mathbf{M^{eS}} = \mathbf{T^{e}}^T \mathbf{M^e} \mathbf{T^e}, \tag{7}$$

and

$$\mathbf{K^{eS}} = \mathbf{T^{e}}^T \mathbf{K^e} \mathbf{T^e}, \tag{8}$$

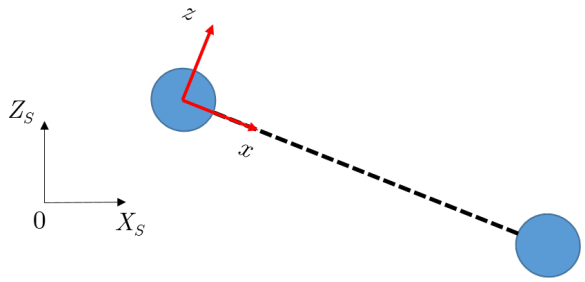

Figure 1: Two-dimensional beam element with arbitrary orientation in the plane.

where ^{T} stands for the transpose and $\mathbf{T^e}$ is the rotation matrix defined as

$$\mathbf{T^e} = \begin{bmatrix} cos(\beta) & sin(\beta) & 0 \\ -sin(\beta) & cos(\beta) & 0 \\ 0 & 0 & 1 \end{bmatrix}, \tag{9}$$

where β is the angle between the local reference frame of each beam element (x,z) and the global axes (X_S,Z_S) (see figure 1).

It is necessary to separate bending DOFs and longitudinal DOFs. Indeed, when those matrices $\mathbf{K^e}$ are computed in the global axes, both DOFs are combined and traction and bending Young's modules are inseparable and also hardly identified.

Eq. (1) can be rewritten to separate, in the stiffness matrix $\mathbf{K}$, the influence of the bending motion and the influence of the flexural motion as

$$\left(\tilde{E}_t\mathbf{K_t} + \tilde{E}_f\mathbf{K_f} - \omega^2\mathbf{M}\right)\mathbf{q} = \mathbf{f}, \tag{10}$$

where $\mathbf{K_t}$ and $\mathbf{K_f}$ represent respectively the assembled stiffness matrices of the longitudinal DOFs and of the transverse DOFs and $\mathbf{M}$ is the assembled mass matrix.

Elimination of force at the boundary of considered area

If the left-hand side of Eq.(10) is evaluated on a part of the structure without external excitation, the vector $\mathbf{f}$ is equal to zero everywhere, except at the boundaries of the considered area. Its non-zero values correspond to two forces and one moment at each extremity. These efforts correspond to reaction forces and moments due to the kinematic continuity between the considered subpart of the structure and the rest of the structure.

To avoid these efforts, the first three lines and the last three lines of matrices $\mathbf{K}_t$, $\mathbf{K}_f$ and $\mathbf{M}$ are removed. Those lines correspond to three DOFs of one node at each extremity of the observed area. If the left-hand side of Eq. (10) is evaluated after this truncation, the resulting forces and moments vanish

on the boundaries, as expected. To keep the notation concise, the truncated matrices will simply be noted $\mathbf{K}_t$, $\mathbf{K}_f$ and $\mathbf{M}$.

Out of the exciting sources, the Eq. (10) becomes

$$\tilde{E}_t \mathbf{K_t q} + \tilde{E}_f \mathbf{K_f q} = \omega^2 \mathbf{M q}. \tag{11}$$

Eq. (11) expresses the equilibrium between the stiffness and the inertia terms, when no external excitation is applied. It should be noted that this equation can be used on a part of the structure, except on parts where external excitation are applied.

Thus, if the displacements $\mathbf{q}$ are known, Young's modules $\tilde{E}_t$ and $\tilde{E}_f$ can theoretically be found using a least square solution of equation

$$\begin{bmatrix} \mathbf{K_t q} & \mathbf{K_f q} \end{bmatrix} \begin{bmatrix} \tilde{E}_t \\ \tilde{E}_f \end{bmatrix} = \omega^2 \mathbf{M q}. \tag{12}$$

Noise on the inverse problem

Taking into account the noise uncertainties due to measurement noise, the observation equation is written as

$$\mathbf{y} = \mathbf{q} + \mathbf{n}, \tag{13}$$

where $\mathbf{y}$ is the vector of observations (or noisy displacements) and $\mathbf{n}$ is the vector of noise. The exact displacement vector $\mathbf{q}$ is actually unknown, only the noisy displacement vector $\mathbf{y}$ is known by measurement. Replacing $\mathbf{q}$ by $\mathbf{y}$ in Eq. (12) makes the least-square approach unstable, because the stiffness terms considerably amplify the noise. Indeed, if this FEM equation of motion is compared to analytical equation of motion, the stiffness term contains high spatial derivative terms, which are particulary sensitive to noise measurement, as discussed by Pézerat in [15]. A regularization step is thus needed.

2.2. Regularization

2.2.1. Principle of the regularization

Considering that the noise is Gaussian, the probability density of noise vector $\mathbf{n}$ can be described as

$$[\mathbf{n}] \sim \mathcal{N}_c(\mathbf{0}, \mathbf{\Sigma_n}), \tag{14}$$

which represents a multivariate complex Gaussian distribution with zero mean value and covariance $\mathbf{\Sigma_n}$ and $\sim$ is the symbol for "is distributed as".

Substituting Eq. (14) in Eq. (13), the probability of exact displacements is

$$[\mathbf{q}|\mathbf{y}, \mathbf{\Sigma_n}] \sim \mathcal{N}_c(\mathbf{y}, \mathbf{\Sigma_n}). \tag{15}$$

It is observed [26] that the calculation of $\mathbf{K_t y}$ and $\mathbf{K_f y}$ is responsible for the instability of the inverse problem, since it drastically amplifies measurement noise. For this reason, the proposed regularization procedure consists in estimating the term

$$\boldsymbol{\delta} = \tilde{E}_t \mathbf{K_t q} + \tilde{E}_f \mathbf{K_f q}. \tag{16}$$

This can be done by merging the probabilistic information provided by two equations. A first equation corresponds to the direct estimation of $\boldsymbol{\delta}$ from noisy displacements by using Eq. (16). Substituting Eq. (15) into Eq. (16) provides the probability density

$$[\boldsymbol{\delta}] \sim \mathcal{N}_c(\tilde{E}_t \mathbf{K_t y} + \tilde{E}_f \mathbf{K_f y}, (\tilde{E}_t \mathbf{K_t} + \tilde{E}_f \mathbf{K_f}) \boldsymbol{\Sigma_n} (\tilde{E}_t \mathbf{K_t} + \tilde{E}_f \mathbf{K_f})^H), \tag{17}$$

where ^{H} indicates hermitian transpose, i.e. the conjugate transpose.

A second equation is related to the verification of the equation of motion Eq. (11), *i.e.*

$$\boldsymbol{\delta} = \omega^2 \mathbf{M q}. \tag{18}$$

Substituting Eq. (15) into Eq. (18) provides the probability

$$[\boldsymbol{\delta}] \sim \mathcal{N}_c(\omega^2 \mathbf{M y}, (\omega^2 \mathbf{M}) \boldsymbol{\Sigma_n} (\omega^2 \mathbf{M})^H). \tag{19}$$

The estimate of $\boldsymbol{\delta}$ can therefore be obtained from the intersection of both probability densities, *i.e.* the product of the two Gaussian distributions of Eqs. (17) and (19),

$$[\boldsymbol{\delta}] \propto \mathcal{N}_c(\boldsymbol{\mu_{\delta_1}}, \boldsymbol{\Sigma_{\delta_1}}) \cdot \mathcal{N}_c(\boldsymbol{\mu_{\delta_2}}, \boldsymbol{\Sigma_{\delta_2}}), \tag{20}$$

where, $\propto$ means "proportional to" and

$$\begin{cases} \boldsymbol{\mu_{\delta_1}} = \tilde{E}_t \mathbf{K_t y} + \tilde{E}_f \mathbf{K_f y} \\ \boldsymbol{\Sigma_{\delta_1}} = (\tilde{E}_t \mathbf{K_t} + \tilde{E}_f \mathbf{K_f}) \boldsymbol{\Sigma_n} (\tilde{E}_t \mathbf{K_t} + \tilde{E}_f \mathbf{K_f})^H \\ \boldsymbol{\mu_{\delta_2}} = \omega^2 \mathbf{M y} \\ \boldsymbol{\Sigma_{\delta_2}} = (\omega^2 \mathbf{M}) \boldsymbol{\Sigma_n} (\omega^2 \mathbf{M})^H \end{cases}. \tag{21}$$

The result itself is a Gaussian distribution,

$$[\boldsymbol{\delta}] \propto \mathcal{N}_c(\boldsymbol{\mu_\delta}, \boldsymbol{\Sigma_\delta}), \tag{22}$$

where the mean vector and covariance matrix are

$$\begin{cases} \boldsymbol{\Sigma_\delta} = \left({\boldsymbol{\Sigma_{\delta_1}}}^{-1} + {\boldsymbol{\Sigma_{\delta_2}}}^{-1} \right)^{-1} \\ \boldsymbol{\mu_\delta} = \boldsymbol{\Sigma_\delta} \left({\boldsymbol{\Sigma_{\delta_1}}}^{-1} \boldsymbol{\mu_{\delta_1}} + {\boldsymbol{\Sigma_{\delta_2}}}^{-1} \boldsymbol{\mu_{\delta_2}} \right) \end{cases}. \tag{23}$$

In the following, the highest value of this gaussian probability density function $[\boldsymbol{\delta}]$, *i.e.* $\boldsymbol{\mu_\delta}$, is considered.

In this section, a regularized estimate of the left hand side of Eq. (11) has been computed.

2.2.2. Definition of a cost function

To perform the identification of Young's modules, the cost function

$$f(\tilde{E}_t, \tilde{E}_f) = \sum |\boldsymbol{\mu_\delta} - \omega^2 \mathbf{M}\mathbf{y}|^2 \tag{24}$$

is introduced, where the dependence on $\tilde{E}_t$ and $\tilde{E}_f$ is carried by $\boldsymbol{\mu_\delta}$ (see Eqs (21) and (23)). The result of this cost function should be theoretically null in the absence of noise, because there is a equality between the mass term and the stiffness terms, as show by Eq. (11).

2.3. Estimation of rotation

A second obstacle to this simple resolution comes from the presence of rotational DOFs in the displacement vector $\mathbf{q}$.

One of the most practical difficulty to implement the proposed approach is that the rotational DOFs in the displacement vector $\mathbf{q}$ must be known. Indeed, theses rotational DOFs cannot be measured directly. A way to estimate them is to use the dynamic condensation method [29]. A condition to use this method is the absence of excitation in the domain where the non-measurable DOFs have to be estimated. This condition is actually verified, because the developed identification technique requires no force and no moment in the domain of interest.

The dynamic condensation consists in partitioning the displacement vector $\mathbf{q}$ into measurable DOFs $\mathbf{q_m}$ (translations) and non-measurable DOFs $\mathbf{q_s}$ (rotations), where subscripts m and s stand for master and slave, respectively. With these notations, Eq. (12) can be rewritten as

$$\left(\tilde{E}_t \begin{bmatrix} \mathbf{K_{t_{mm}}} & \mathbf{K_{t_{ms}}} \\ \mathbf{K_{t_{sm}}} & \mathbf{K_{t_{ss}}} \end{bmatrix} + \tilde{E}_f \begin{bmatrix} \mathbf{K_{f_{mm}}} & \mathbf{K_{f_{ms}}} \\ \mathbf{K_{f_{sm}}} & \mathbf{K_{f_{ss}}} \end{bmatrix} - \omega^2 \begin{bmatrix} \mathbf{M_{mm}} & \mathbf{M_{ms}} \\ \mathbf{M_{sm}} & \mathbf{M_{ss}} \end{bmatrix} \right) \begin{Bmatrix} \mathbf{q_m} \\ \mathbf{q_s} \end{Bmatrix} = \begin{Bmatrix} \mathbf{0_m} \\ \mathbf{0_s} \end{Bmatrix}. \tag{25}$$

Using the second line of Eq. (25),

$$\left[\tilde{E}_t \mathbf{K_{t_{sm}}} + \tilde{E}_f \mathbf{K_{f_{sm}}} + \omega^2 \mathbf{M_{sm}}\right] \mathbf{q_m} + \left[\tilde{E}_t \mathbf{K_{t_{ss}}} + \tilde{E}_f \mathbf{K_{f_{ss}}} + \omega^2 \mathbf{M_{ss}}\right] \mathbf{q_s} = \mathbf{0_s}, \tag{26}$$

it is possible to estimate the unknown rotations $\mathbf{q_s}$ from the translations $\mathbf{q_m}$ as

$$\mathbf{q_s} = \mathbf{C} \cdot \mathbf{q_m}, \tag{27}$$

with,

$$\mathbf{C} = - \left[\tilde{E}_t \mathbf{K_{t_{ss}}} + \tilde{E}_f \mathbf{K_{f_{ss}}} - \omega^2 \mathbf{M_{ss}} \right]^* \left[\tilde{E}_t \mathbf{K_{t_{sm}}} + \tilde{E}_f \mathbf{K_{f_{sm}}} - \omega^2 \mathbf{M_{sm}} \right], \tag{28}$$

where * means a pseudo-inverse [30].

It should be noted that Eq. (26) provides $(N-2)$ scalar equations, which is due to the fact that the moment is null everywhere, except at the boundary nodes (as discussed in section 2.1). Hence, the estimation of N rotations from Eq. (26) is slightly under-estimated. An example of rotation computation is illustrated in section 3.2.

2.4. Probability of exact displacements

The displacement vector $\mathbf{q}$ has three kind of components, the translations along the X_S and the Z_S directions and the rotations. The two first quantities are regrouped in the vector $\mathbf{q_m}$ and are directly measured, whereas the rotations $\mathbf{q_s}$ are estimated from vector $\mathbf{q_m}$.

The probability of exact translations $[\mathbf{q_m}|\mathbf{y_m}, \sigma_n^2]$ is given from Eq. (15), with σ_n^2 a scalar variance of noise for the translations,

$$[\mathbf{q_m}|\mathbf{y_m}, \sigma_n^2] \sim \mathcal{N}_c(\mathbf{y_m}, \sigma_n^2 \cdot \mathbf{I}), \tag{29}$$

where $\mathbf{I}$ stands for the identity matrix.

When Eq. (29) is substituted in Eq. (27), the probability of exact rotations is

$$[\mathbf{q_s}|\mathbf{C}, \mathbf{y_m}, \sigma_n^2] \sim \mathcal{N}_c\left(\mathbf{q_s}|\mathbf{C}\mathbf{y_m}, \mathbf{C}\sigma_n^2\mathbf{C}^H\right). \tag{30}$$

Eqs. (29) and (30) can be concatenated to build the probability $[\mathbf{q}]$ as,

$$[\mathbf{q}|\mathbf{y}, \sigma_n^2, \mathbf{\Sigma_q}] \sim \mathcal{N}_c\left(\mathbf{q}|\mathbf{y}, \sigma_n^2\mathbf{\Sigma_q}\right), \tag{31}$$

with,

$$\mathbf{y} = \begin{bmatrix} \mathbf{y_m} \\ \mathbf{y_s} \end{bmatrix}, \tag{32}$$

$$\mathbf{\Sigma_q} = \begin{bmatrix} \mathbf{I} & \mathbf{0} \\ \mathbf{0} & \mathbf{C}\mathbf{C}^H \end{bmatrix}. \tag{33}$$

The Eq. (21) can be rewritten as

$$\begin{cases} \boldsymbol{\mu_{\delta_1}} = \tilde{E}_t\mathbf{K_t}\mathbf{y} + \tilde{E}_f\mathbf{K_f}\mathbf{y} \\ \mathbf{\Sigma_{\delta_1}} = (\tilde{E}_t\mathbf{K_t} + \tilde{E}_f\mathbf{K_f})\sigma_n^2\mathbf{\Sigma_q}(\tilde{E}_t\mathbf{K_t} + \tilde{E}_f\mathbf{K_f})^H \\ \boldsymbol{\mu_{\delta_2}} = \omega^2\mathbf{M}\mathbf{y} \\ \mathbf{\Sigma_{\delta_2}} = (\omega^2\mathbf{M})\sigma_n^2\mathbf{\Sigma_q}(\omega^2\mathbf{M})^H \end{cases}. \tag{34}$$

It can be shown from Eqs. (34) and (23) that $\boldsymbol{\mu_\delta}$ finally does not depend on σ_n. The evaluated expression does not contain parameter of regularization, which has to be adjusted by a method such as L-curve or Generalized Cross Validation (GCV), as discussed by Faure [31].

2.5. Numerical implementation of the identification method

To resume the main steps of the developed method, the first step is to build the FE matrices of the subpart of the system ($\mathbf{M}$, $\mathbf{K_T}$ and $\mathbf{K_F}$) for which the structural parameters are looking for. This building is done from the geometrical dimensions of the beam and from the density of the material.

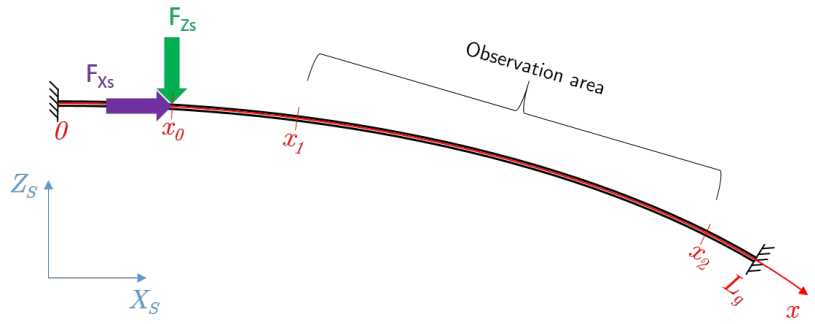

Figure 2: Geometry of beam used for numerical simulation.

Then those square matrices are truncated by removing 6 lines, to avoid bonding efforts coming from the rest of the structure.

The second step is to obtain the translation field $\mathbf{y_m}$ for each frequency, either by measurement, for example with a scanning laser vibrometer, or by numerical simulations, for example to test the method.

The following steps are part of the minimization procedure to obtain the complex Young's modules and are done for each frequency. In a first part, after initializing the complex Young's modules, the rotations $\mathbf{y_s}$ are estimated with the dynamic condensation procedure from Eq. (27). In a second part, the translations and the rotation are concatenated in the vector $\mathbf{y}$ from Eq. (32). In a third part, the variance $\mathbf{\Sigma_q}$, from Eq. (33), and the MAP $\boldsymbol{\mu_\delta}$, from Eq.(23), are computed. And in a fourth and last part, the cost function is minimized by repeating all these steps from Eq.(24).

Finally, the complex Young's modules $\tilde{E}_t^{freq}$ and $\tilde{E}_t^{freq}$ are thus obtained. The superscript ^{freq} means that Young's modules depends on the frequency and that they have to be determined for each frequency.

The main steps of the developed method are condensed in the algorithm given in the Appendix A.

3. Numerical simulation

3.1. Direct problem

In this section, the reference solution is calculated using the FEM. Let us consider a clamped-clamped isotropic beam (figure 2), with a curvature of 1 m and whose characteristics are given in Table 1. The beam is simultaneously excited in the both direction X_S and Z_S.

The displacements $\mathbf{q}$ are computed at discrete abscissas delimited by $x \in [0.3; 0.8]$ m, region without excitation. The translations and the rotations are plotted in figure 3.

Geometric parameters	Length L_g (m)	1
	Width b (m)	0.01
	Thickness h (m)	0.001
	Second Moment of Area I_z (m^4)	$bh^3/12$
	Spatial sampling Le (m)	0.01
	Curvature radius R (m)	1
Material parameters	Density ρ (kg/m^3)	2700
	Traction Young's modulus E_t (GPa)	75
	Traction loss factor η_t	0.1 %
	Bending Young's modulus E_f (GPa)	70
	Bending loss factor η_f	0.1 %
Excitation characteristics	Frequency (Hz)	500
	Excitation force $\lvert F_{X_S}\rvert = \lvert F_{Z_S}\rvert$ (N)	1
	Excitation location x_0 (m)	0.1
Observation area $[x_1; x_2]$ (m) in curvilinear axes		$[0.3; 0.8]$

Table 1: Geometrical and material properties set for the simulated beam and excitation characteristics.

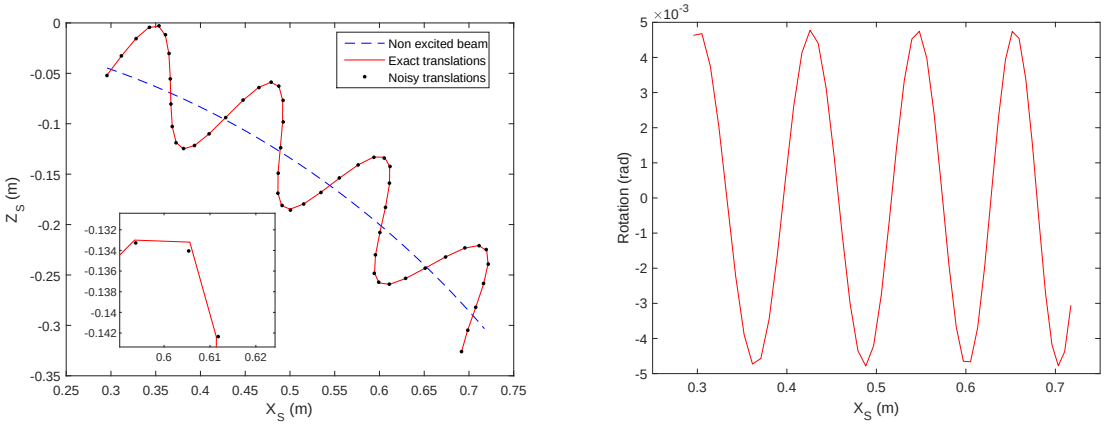

(a) (b)

Figure 3: Displacements in observation area: (a) Translations (magnified with a scaling factor of 10'000) in the global axes without noise and noisy (SNR = 35 dB), (b) Rotation in the global axes of the beam.

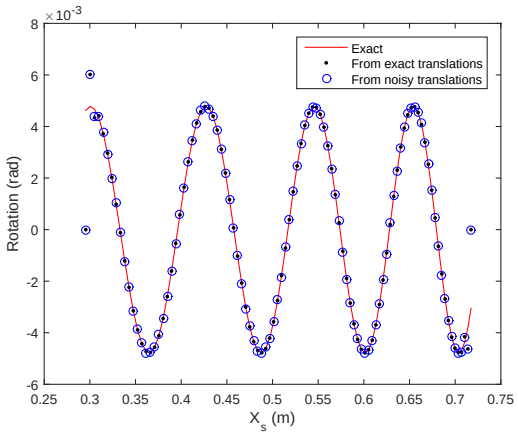

Figure 4: Reconstruction of rotation (–) by dynamic condensation: from exact simulated translations (•) and from noisy simulated translations (○).

To approximate a measurement, the translations previously calculated, are blurred with noise,

$$\mathbf{y_m} = \mathbf{q_m} + 10^{\frac{-SNR}{20}}\alpha, \tag{35}$$

with $\mathbf{y_m}$, the noisy translations, SNR, the Signal to Noise Ration and α, a zero mean Gaussian random variable with unit variance. Noisy translations are also shown in figure 3 (a) with a SNR equal to 35 dB.

3.2. Illustration of rotation computation

A first step is to verify the rotations computed by dynamic condensation from exact translations $\mathbf{q_m}$ using Eq. (27). Black points in figure 4 are obtained. The computed rotations are in accordance with exact rotations in red solid line in figure 4, except near the boundaries of the studied area. This is a consequence of the under-determined nature of Eq. (26). That is why the point at each extremity cannot be determined. By default, it is set to zero. These false value is propagated to the nearest point. For this reason, two nodes at each extremity of the area will be used only for the rotations estimation. This four nodes will not be considered in the final material characterization.

A second step is to test the reconstruction of the rotation from noisy translations. The blue circles in figure 4 represent the rotations obtained from Eq. (27) with noisy translations $\mathbf{y_m}$. It can be observed that they are very close to the rotations estimated from exact translations, which shows that the estimation of rotations is not very sensitive to measurement noise.

3.3. Identification of both traction and bending complex Young's modules

3.3.1. Simulation of an aluminum beam

The results of identification of Young's modules are illustrated for the frequency of 500 Hz. Figure 5 (a) shows the cost function defined in Eq. (24). Using exact displacements $\mathbf{q}$, a minimum of the

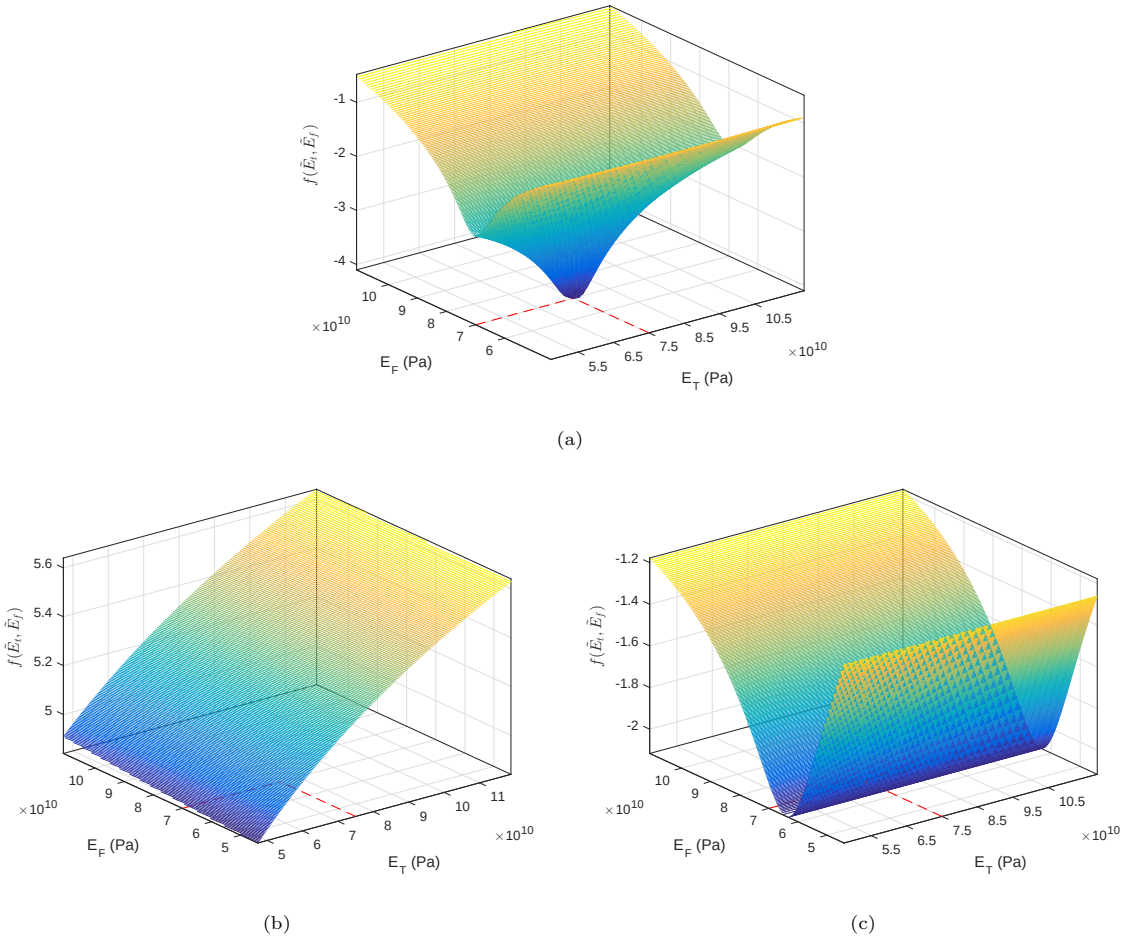

Figure 5: Cost function depending of the traction and the bending Young's modules (E_t, E_f) for: (a) exact data, (b) noisy data without regularization and (c) noisy data with regularisation.

cost function is clearly obtained at the correct values of Young's modules.

This first case with exact translations is also computed for a large frequency band with the regularization process (see Appendix A). The identification results are given in figure 6.

Figure 6 (a) shows the identification of the Young's modules. It can be seen the bending Young's modulus is identified for all frequencies, at its value of 70 GPa. The identification of the traction Young's modulus is near its value of 75 GPa, for the high frequencies. Before 8 kHz, some singularities are observed. The identification of the traction modulus is very sensitive, because the involved translations are very small, especially at low frequencies, where no resonances are present, and also the regularization process brings noise, which disturbs this identification. The same results for loss factors are visible in figure 6 (b). The bending loss factor are identified for all frequencies, while traction loss factor identification let see some singularities, especially at low frequencies.

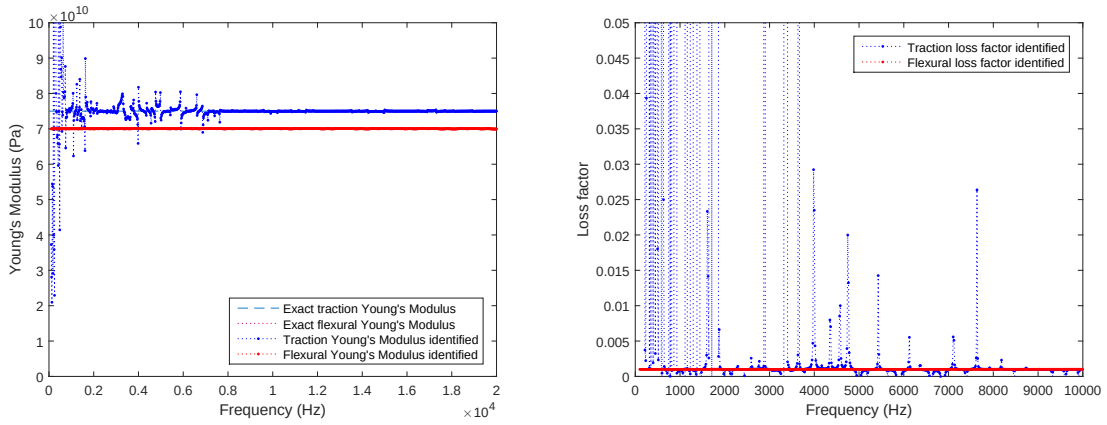

(a) (b)

Figure 6: Identification results on the simulated aluminum beam from exact translations with the regularization process: (a) Young's modules and (b) loss factors.

When noise is added to translations, the cost function obtained are shown in figure 5 (b). It can be observed that Young's modules cannot be identified.

After regularisation, it appears in figure 5 (c), that the cost function is much more sensitive to variations in flexural Young's modulus E_f than in traction Young's modulus E_t. To verify that both Young's modules can be still identified, a minimization technique is applied to this cost function for a large band of frequencies, between 100 Hz and 20 kHz.

Figure 7 (a) and (b) show the result of the parameters identification with a SNR set to 35 dB.

It can be observed that the bending Young's modulus is correctly identified at almost all frequencies. For the traction/compression Young's modulus, the identification seems to be more difficult, especially in the low frequency domain. A plausible explanation is that traction/compression wavelength is too large compared to the length of the considered area before the second mode of traction, which occurs around 7.5 kHz. Figure 7 (b) shows the extreme difficulty to obtain accurate results for traction/compression and bending loss factor, when the structural damping is small.

In order to show the sensitivy of the method to different noise ratio, figure 7 (c) and (d) present the result of the parameters identification with a SNR fixed to 20 dB. It is then observed the same behavior about Young's modules identification. Indeed, the bending Young's modulus (figure 7 (c)) is correctly identified to its value of 70 GPa, but the traction Young's modulus shows difficulties to be identified especially at low frequencies. Nevertheless, a drop of SNR allows a better identification even at low frequencies of this structural parameter. For the loss factors identification, figure 7 (d), it can be observed a better identification when the SNR is lower. It is noticed the bending loss factor is correctly identified around its value of 0.1 % and the traction loss factor is not identified to its value

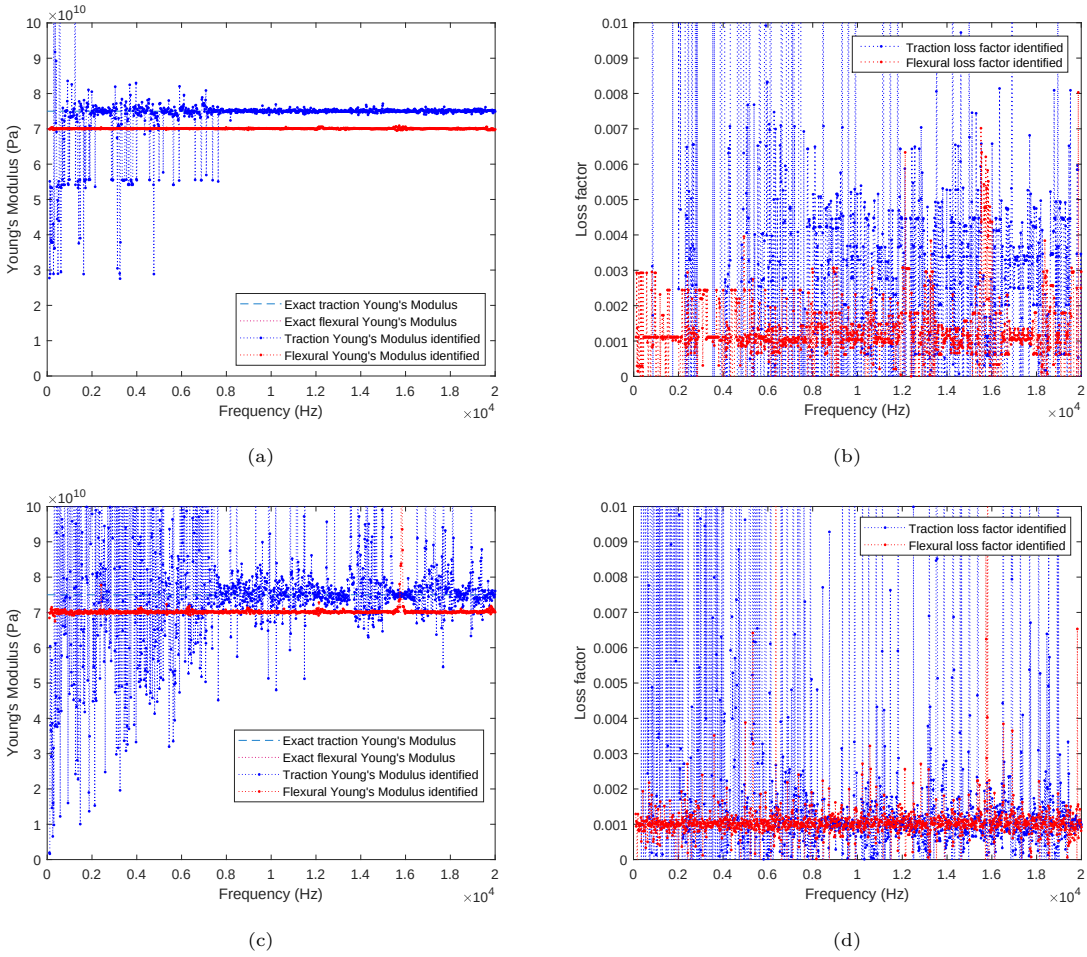

Figure 7: Identification of complex Young's modules for a large frequency band for a simulated beam, with SNR = 35 dB: (a) Young's modules in traction/compression and in bending movement, (b) Loss factors in traction/compression and in bending and with SNR = 20 dB: (c) Young's modules in traction/compression and in bending movement, (d) Loss factors in traction/compression and in bending.

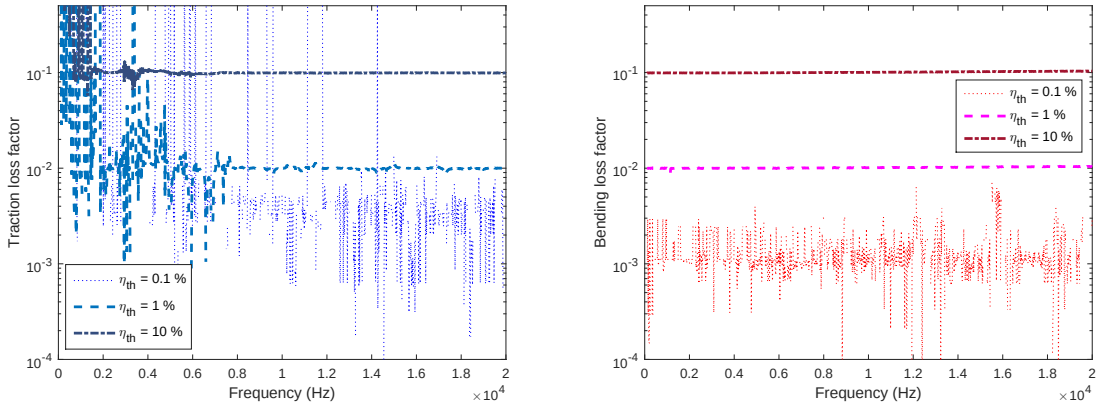

(a) (b)

Figure 8: Loss factor identification sensitivity through the simulation of an aluminum beam with different loss factors: 0.1 %, 1 % and 10 %. Identification of (a) traction loss factor and (b) bending loss factor.

of 0.1 %.

3.3.2. Loss factor identification sensitivity

In the previous section, it has been observed that loss factors identification seems to be very sensitive. In this section, it is proposed to study this sensitivity. Three cases of translations are simulated for the same aluminum beam, but with three different loss factors: 0.1 %, 1 % and 10 % and the SNR of translations is fixed to 35 dB. Loss factors identifications are presented in figure 8 (a) for the traction loss factors identifications and in figure 8 (b) for the bending loss factors identifications.

It can be observed for those both figures a better identification when the loss factor increases. Indeed, higher are the loss factors, more influence they have on the beam motion, and more correctly they are identified.

3.3.3. Preliminary conclusion for structural identification from simulated cases

In this part, identification results from simulated cases were presented. Preliminary conclusions can be done in order to explain further identification of complex modules with this method.

The first one concerns the identification of Young's modules. It has been observed that the bending Young's modulus is easier to identify than the traction Young's modulus, especially at low frequencies. This difficulty to identify traction parameters comes from the difference of behavior between bending and traction motion. Indeed, the wavelengths involved between those two movements are drastically different and this has two consequences: the measured area can be too small to capture a sufficient portion of traction wavelength and the level of traction translations is very low when few modes are involved.

The second concerns the identification of loss factors. As with Young's modulus identification, it has been shown that it is easier to identify bending Young's modulus than traction Young's modulus, especially at low frequencies. Furthermore, a high loss factor is easier to identify. It can be explained, because a small loss factor has less influence on the beam motion.

4. Experimental Results

This section presents experimental results obtained on two beams :

- an aluminum straight beam,
- a sandwich curved beam.

In all experiments, the structure has one extremity free and the other driven by a shaker (LDS V201). The shaker was equipped with a force sensor (PCB 208C02). The excitation signal was a periodic chirp between 100 Hz and 20 kHz. This shaker is recommended to work between 5 Hz and 13 kHz. In these cases, it is used up to 20 kHz, but the input signal has been reworked to obtain a sufficient excitation level and the coherence is verified over the whole frequency band. Two kind of excitation can be used, one excites predominantly the longitudinal direction (following X_S) and the second excites predominantly the transverse direction (following Z_S). The vibratory field was measured using the measurement platform 3D Vib, a Polytec 3D scanning vibrometer (Polytec PSV-500-3D-xtra) mounted on an industrial robot. The translations were measured on a meshgrid constituted of five points along the width of the beam. 730 points are measured. Traction and flexural translations of these five points are averaged in order to have a value at each abcissa along the beam and to reduce the measurement noise. The distance between points in length and in width is fixed to 3.33 mm.

4.1. Experimental validation on aluminum straight beam

The first experiment concerns the aluminum beam. The beam has a length of 0.5 m, a width $b = 0.02$ m and a thickness $h = 0.002$ m. The mass density of the beam is 2700 kg.m^{-3}. The section of the beam is also a rectangle, so the second moment of area is calculated by $I_z = \frac{bh^3}{12}$. This beam is excited principally by a longitudinal excitation (following X_S).

The measured mobility of the beam is presented in figure 9. The dashed blue line represents the mobility of the beam along the X_S-axis. Four peaks are observed, which show four resonances of traction. The yellow line represents the mobility of the beam along the Z_S-axis. On this one, a lot of bending resonance are visible. A difference of behavior between traction and bending movements is also noted, since the involved wavelengths are not the same.

Using the algorithm presented in Appendix A and initializing $\tilde{E}_t^0$ and $\tilde{E}_f^0$ to $50(1 + 1j)$ GPa, identification results are shown in figure 10. The traction Young's modulus is successfully identified

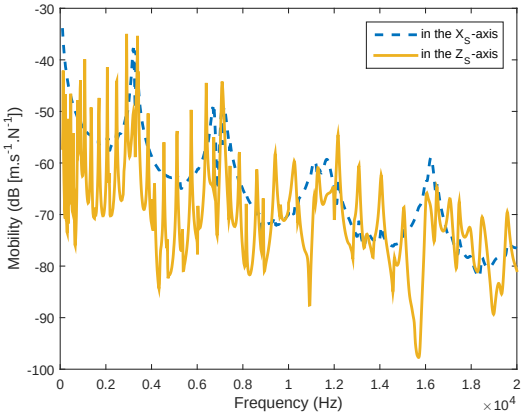

Figure 9: Averaged mobility of the aluminum straight beam in the three direction for an excitation along the X_S-axis.

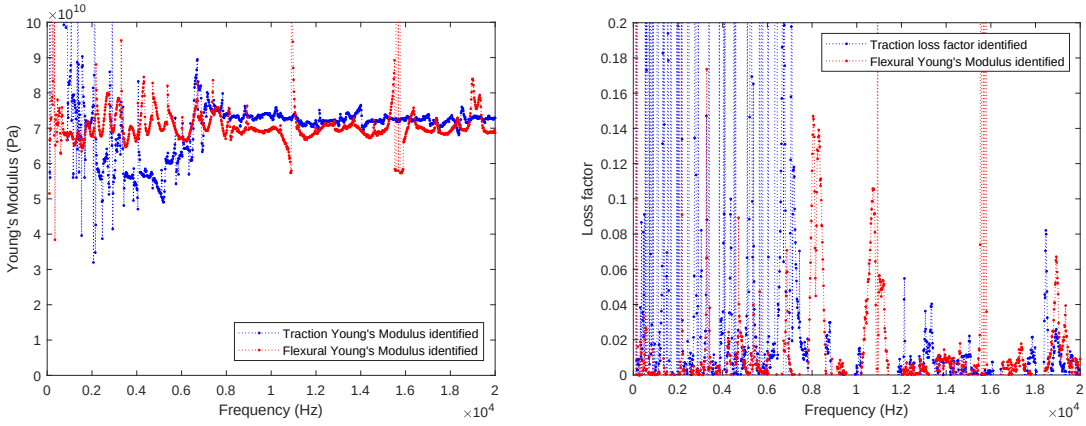

(a) (b)

Figure 10: Identification on an aluminum straight beam between 100 Hz and 20 kHz: (a) Traction and flexural Young's modules ; (b) Traction and flexural loss factors.

from 8 kHz to 20 kHz and its value is around 72 GPa. Before 8 kHz, there is not enough amplitude associated to the traction/compression motion of the beam.

The flexural Young's modulus is clearly identified after 2 kHz, but its value oscillates between 60 and 80 GPa. After 7 kHz, when the traction Young's modulus seems correctly identified, the value of flexural Young's modulus is more stable with a mean value 68 GPa.

The values of Young's modules after 8kHz are in accordance with the aluminum material, which typically has a Young's modulus around 70 GPa.

As usual results with this kind of inverse method, loss factors are hardly identifiable, because it has a very low value for aluminum material. In figure 10 (b), traction and flexural loss factors can not be identified.

4.2. Identification on sandwich curved beam

The second experiment concerns the sandwich curved beam, as shown as figure 11. The sandwich material is composed of two steel skins of 1 mm each and a resin core of 0.04 mm, so that the total thickness of the beam is $h = 2.04$ mm. The mass density is calculated and gives 7666 kg.m^{-3}.

The geometry of the beam consists of two straight portions, forming an angle of 50° and linked by a curved portion with a curvature radius of 0.150 m. The length of the beam is 0.5 m. The section is rectangular too, with a width $b = 0.02$ m.

The measured area has a length close to 0.485 m. It covers about 97 % of the total length and fully includes the curved portion.

In this part, two kind of excitation are studied : an excitation along the X_S-axis and an excitation along the Z_S-axis. The averaged mobility of the curved sandwich beam in the three directions is plotted in figure 12 for each excitation.

For this identification, traction Young's modulus initialization is fixed to $150(1 + 1j)$ GPa and bending Young's modulus to $70(1 + 1j)$ GPa. Figure 14 shows the results of the identification with the proposed inverse method.

Firstly, results for the excitation along the X_S-axis are described and commented. The homogenized traction Young's modulus, in figure 14 (a), is clearly identified after 1800 Hz. Its value is around 220 GPa, which is close to the value for steel. Indeed traction motion is governed by the skins of the sandwich, the resin core is only slightly solicited by this motion. In consequence, traction loss factor (in figure 14 (b)) is hard to identify because it is very low, less than 0.1 %. That corresponds to steel loss factor.

Regarding homogenized flexural Young's modulus, in figure 14 (a), its identification seems to be more complicated. At low frequencies, a fall of its value is observed from 200 GPa to around 100 GPa. Between 2 kHz and 5.5 kHz, 11 kHz and 13.5 kHz and 14.7 and 18.4 kHz, this value is monotone

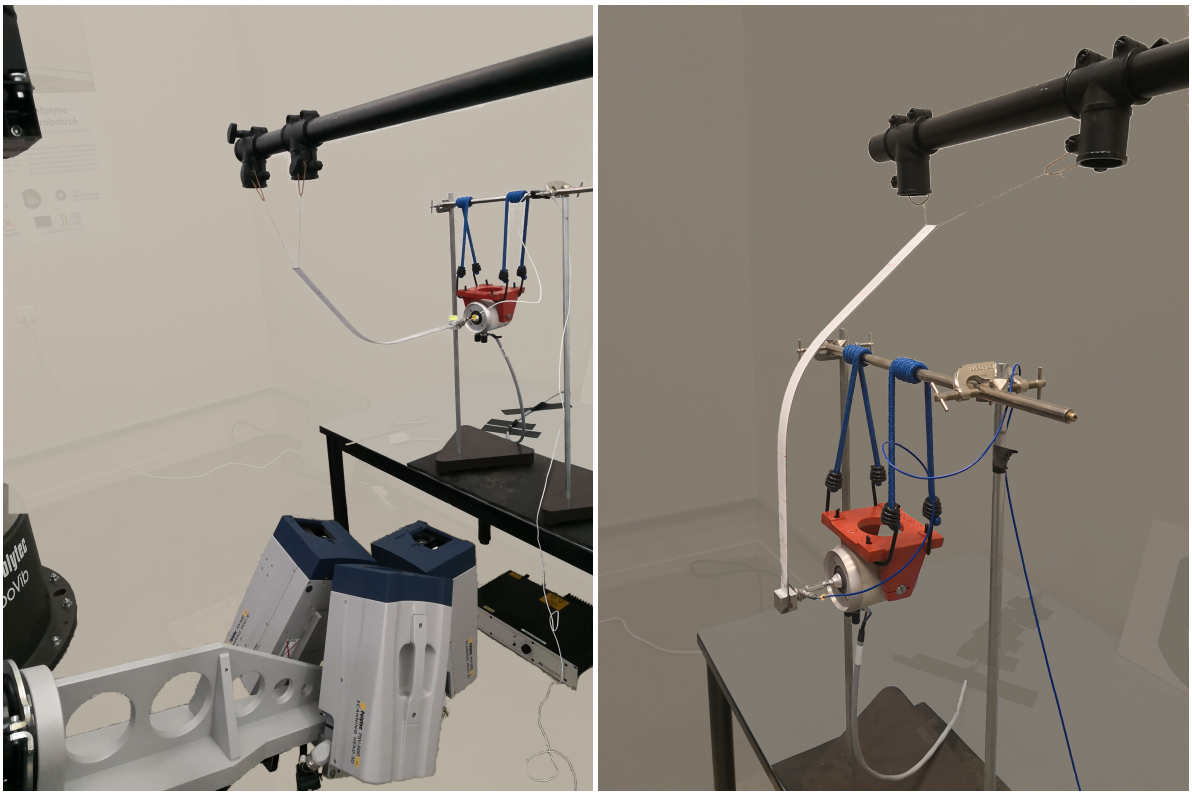

(a) (b)

Figure 11: Experimental setup for translations measurements of a curved sandwich beam with a 3D Scanning Vibrometer on a robot for (a) an excitation along the X_S-axis and (b) an excitation along the Z_S-axis.

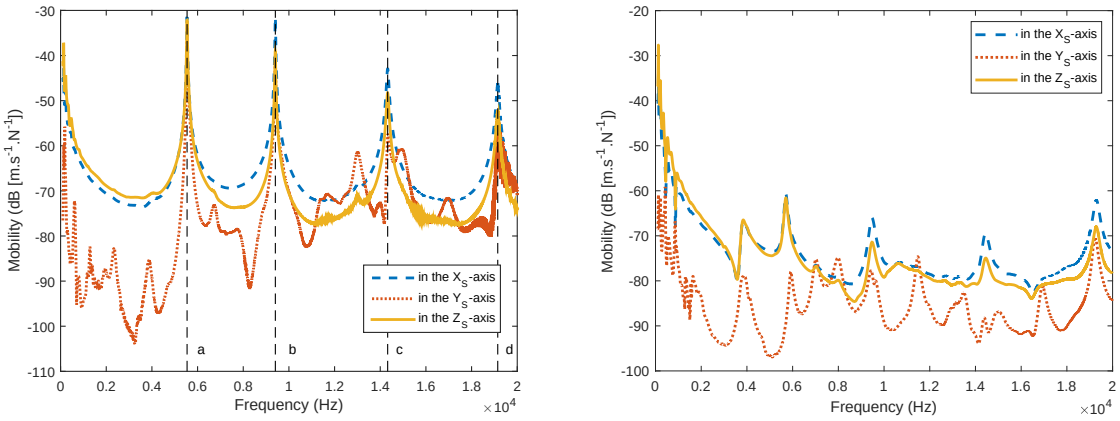

(a) (b)

Figure 12: Averaged mobility of the curved sandwich beam in the three directions for (a) an excitation along the X_S-axis and (b) an excitation along the Z_S-axis.

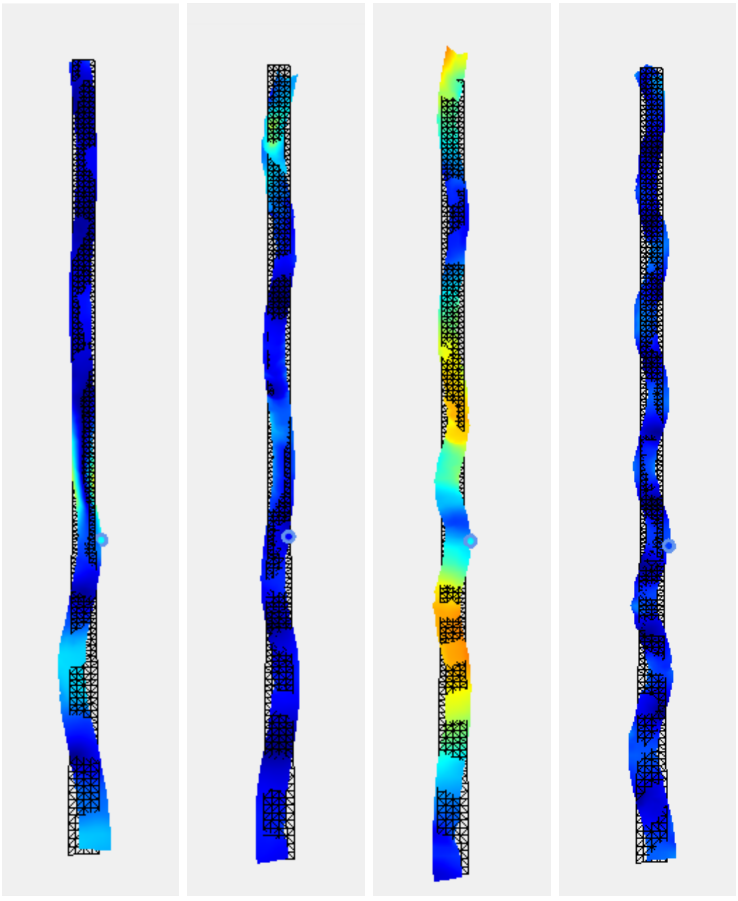

(a) 5540 Hz (b) 9406 Hz (c) 14325 Hz (d) 19146 Hz

Figure 13: Operational deflection shapes of the sandwich curved beam excited along the X_S-axis, for four frequencies : (a) at 5540 Hz, (b) at 9406 Hz, (c) at 14325 Hz and (d) at 19146 Hz

and decreases slowly. Sandwich structures involve shearing motion. The developped model neglects this kind of motion. In consequence the apparent Young's modulus lowers [32]. This identification procedure fails for three frequency bands : between 6 and 11 kHz, around 14 kHz and around 19 kHz. As it can be seen on figure 12 (a), for each frequency band, other motions (twist or lateral bending) appear, which are not taken into account in the finite element model of the inverse problem. The mode shapes of the beam for these frequencies are given in figure 13. Flexural loss factor (in figure 14 (b)) is also clearly identified, except for traction modes frequencies. The flexural loss factor is higher than 20 % before 6 kHz and around 15 % after this frequency. This relatively high loss factor is due to viscoelasticity of the resin, which is expected to provide high damping.

Secondly, results for the excitation along the Z_S-axis are described and commented. Homogenized traction Young's modulus seems to be more difficult to identify before 14 kHz, in figure 14 (c), even if this mean value is around 225 GPa. After 14 kHz, its identification is more stable. In figure 14 (d),

the homogenized traction loss factor is always hard to identify, due to its low value.

However, homogenized flexural Young's modulus, in figure 14 (c), is better identified than the excitation is along the axis X_S. The same decrease is observed at low frequencies, but the identification failures are more limited on the flexural Young's modulus, as well as on the homogenized loss factor, in figure 14 (d). This behavior of the homogenized loss factor is a common result for laminated structures as for example shown by Manconi [33]. Indeed for laminated structures, loss factor value presents a bell-shaped curve. It means at low frequencies a low value of loss factor, then a rise up to a peak and after a drop of its value.

It can be concluded comparing both results for different directions of excitation, that the excitation conditions the result of the identification. If two complex modules are sought with only one measurement, a compromise between an excitation along the X_S-axis and along the Z_S-axis should be found to excite properly the motion of traction and the motion of bending.

5. Conclusion

This paper presents an inverse method to identify traction and flexural stiffnesses of a curved beam. The developed method is based on the FAT method coupled to a Finite Element operator to replace the need of the analytical dynamic motion equation.

The application of this method requires the knowledge of the structure geometry, which allows to build stiffness and mass matrices. Other conditions are the absence of external effort on the measured area and the access of the translation field. In the present case, two components of the displacement are required, the traction and the flexural translations. The sensitivity to measurement noise is overcome by a probabilistic approach, which adjusts automatically the level of regularization. A dynamic condensation method is used to compute from the translations the flexural rotation.

The method has been validated experimentally on an aluminum straight beam and on a sandwich curved beam. For those both cases, traction and bending Young's modules were identified on a wide frequency band between 100 Hz and 20 kHz. For aluminum beam, loss factors are too low to be well identified. However for sandwich beam, bending loss factor is clearly identified.

Through different simulations and experiments, some good practices can be deduced to apply this method to a curved beam. Firstly, the measurement is a very important point for two main reasons. Inverse methods are sensitive to noise and also needs denoising procedure. A way to have a correct result is to have a SNR as low as possible. The second reason concerns the excitation. In this paper, it is shown that the beam have to be sufficiently excited in the direction of the traction and in the direction of the bending to identify correctly the structural parameters. Moreover, it has been observed that the traction Young's modulus is more difficult to obtain than bending Young's modulus. That's

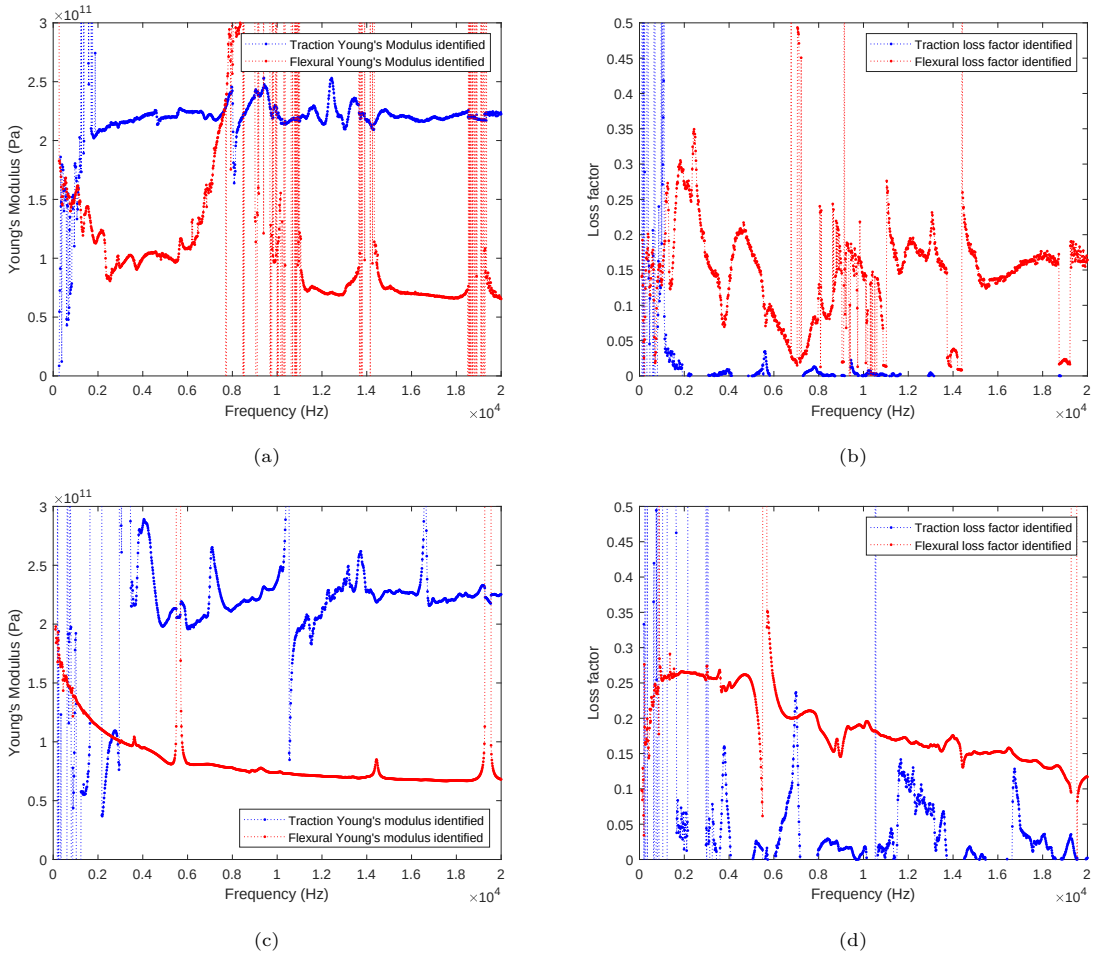

Figure 14: Identification on a sandwich curved beam of between 100 Hz and 20 kHz: (a) Bending and flexural Young's modulus and (b) Bending and flexural loss factor, for an excitation along the X_S-axis; (c) Bending and flexural Young's modulus and (d) Bending and flexural loss factor, for an excitation along the Z_S-axis

why, it would be necessary to pay special attention to the direction of the excitation. Furthermore, it has been noted that others motions can occur and disturb the identification at particular frequencies, as seen for bending Young's modules, which are disturbed by twist motion. These others movements, which are not taken into account in the model, can be limited by an excitation as clean as possible.

Secondly, for the identification procedure, an attention should be taken to the initialization of the Young's modules. It can be suggested an improvement to initialize the minimization procedure in determining the Young's modules by static methods (Dynamic Mechanical Analyses for example) to have an idea of the Young's modules and to use those values as initialization values.

The third recommendation concerns the limit about loss factor identification. With this presented method, it can be concluded that low loss factors cannot be determined by this method, because they don't have enough influence on the beam motion and the information is lost in the measurement noise. Nevertheless, that doesn't prevent to identify correctly Young's modules.

A last point can also be discussed, the choice of the FE model. Some studies were already done by Wassereau [18, 32] on thick beams and by Ruzek on the selection of vibration models [34, 35], and a deeper study would be necessary about the choice of this FE model. Indeed, refined models describe more accurately the structure dynamics, but have lower robustness when using an inverse method. This is the reason why we use here a simple FE model, which will depict the right dynamics for the global beam. However this model can be more complex to describe the local strain and stress inside the beam section.

Acknowledgements

This study is part of the RICTUS project managed by IRT Jules Verne (French Institute in Research and Technology in Advanced Manufacturing Technologies for Composite, Metallic and Hybrid Structures), supported by Safran, Valeo and CETIM.

Appendix A Algorithm of the inverse problem

Require: Initialize : $\tilde{E}_t^0$, $\tilde{E}_t^0$

$\mathbf{M}, \mathbf{K_T}, \mathbf{K_F} \leftarrow$ compute FE matrices

for $freq \in [freq_{min}, freq_{max}]$ **do**

  $\mathbf{y_m} \leftarrow$ get the translations field at frequency f

  $\mathbf{y_s} \leftarrow$ calculate from Eq. (27), $\tilde{E}_t^{i-1}$ and $\tilde{E}_f^{i-1}$

  $\mathbf{y} \leftarrow$ calculate from Eq. (32)

  $\mathbf{\Sigma_q} \leftarrow$ calculate from Eq. (33)

  $\boldsymbol{\mu_\delta} \leftarrow$ calculate from Eq.(23)

  $\tilde{E}_t^i, \tilde{E}_f^i \leftarrow$ obtain in minimizing $f(\tilde{E}_t, \tilde{E}_f)$ from Eq.(24)

  $\tilde{E}_t^{freq} \leftarrow \tilde{E}_t^N$ (see Figure 7)

  $\tilde{E}_f^{freq} \leftarrow \tilde{E}_f^N$ (see Figure 7)

end for

References

[1] K. P. Menard, Dynamic Mechanical Analysis: A Practical Introduction, 2nd Edition, CRC Press, 2008.

[2] D. J. Ewins, Modal Testing: Theory, Practice and Application, 2nd Edition, Research Studies Press, 2000.

[3] E. Fotsing, M. Sola, A. Ross, E. Ruiz, Dynamic characterization of viscoelastic materials used in composite structures, Journal of Composite Materials 48 (30) (2014) 3815–3825. arXiv:https://doi.org/10.1177/0021998313514254, doi:10.1177/0021998313514254.
URL https://doi.org/10.1177/0021998313514254

[4] A. E756, Standard test method for measuring vibration-damping properties of materials (1998).

[5] D. Montalvão, R. Cláudio, A. Ribeiro, J. Duarte-Silva, Experimental measurement of the complex young's modulus on a cfrp laminate considering the constant hysteretic damping model, Composite Structures 97 (2013) 91 – 98. doi:https://doi.org/10.1016/j.compstruct.2012.10.050.
URL http://www.sciencedirect.com/science/article/pii/S026382231200551X

[6] V. Palan, W. S. Shepard, J. G. McDaniel], Characterization of an experimental wavenumber fitting method for loss factor estimation using a viscoelastically damped structure, Journal of Sound and Vibration 291 (3) (2006) 1170 – 1185. doi:https://doi.org/10.1016/j.jsv.2005.07.028.
URL http://www.sciencedirect.com/science/article/pii/S0022460X05004918

[7] P. Blaschke, T. Schneider, Reactionless Test to Identify Dynamic Young's Modulus and Damping of Isotropic Plastic Materials, Springer New York, New York, NY, 2014, pp. 511–516. doi:10.1007/978-1-4614-6585-0_49.
URL http://dx.doi.org/10.1007/978-1-4614-6585-0_49

[8] E. Barkanov, E. Skukis, B. Petitjean, Characterisation of viscoelastic layers in sandwich panels via an inverse technique, Journal of Sound and Vibration 327 (3) (2009) 402 – 412. doi:https://doi.org/10.1016/j.jsv.2009.07.011.
URL http://www.sciencedirect.com/science/article/pii/S0022460X09005835

[9] C. Potel, T. Chotard, J.-F. de Belleval, M. Benzeggagh, Characterization of composite materials by ultrasonic methods: modelization and application to impact damage, Composites Part B: Engineering 29 (2) (1998) 159 – 169, high Temperature Composites and Interfaces: Analysis, Processing and Characterization. doi:https://doi.org/10.1016/S1359-8368(97)00006-1.
URL http://www.sciencedirect.com/science/article/pii/S1359836897000061

[10] P. Bodian, P. Guy, B. Chassignole, O. Dupond, L. Doudet, Évaluation non destructive des propriétés d'élasticité et d'atténuation ultrasonore dans des matériaux anisotropes (non-destructive assessment of elasticity and ultrasonic attenuation properties in anisotropic materials), Congrès Français d'Acoustique (CFA) (2010).

[11] M. Grédiac, Principe des travaux virtuels et identification. (principle of virtual work and identification), Comptes Rendus de l'Académie des Sciences. Série II 309 (01 1989).

[12] A. Giraudeau, F. Pierron, Identification of stiffness and damping properties of thin isotropic vibrating plates using the virtual fields method: Theory and simulations, Journal of Sound and Vibration 284 (2005) 757–781. doi:10.1016/j.jsv.2004.07.009.

[13] F. Pierron, G. Vert, R. Burguete, S. Avril, R. Rotinat, M. R. Wisnom, Identification of the orthotropic elastic stiffnesses of composites with the virtual fields method: Sensitivity study and experimental validation, Strain 43 (2007) 250 – 259. doi:10.1111/j.1475-1305.2007.00346.x.

[14] C. Pézerat, Method of identification of forces applied on a vibrating structure, by resolution and regularization of the inverse problem, Ph.D. thesis, INSA de Lyon (Dec. 1996).
URL https://tel.archives-ouvertes.fr/tel-00778516

[15] C. Pézerat, J.-L. Guyader, Two inverse methods for localization of external sources exciting a beam, in: Acta Acustica, Vol. 3, 1995, pp. 1–10.

[16] C. Pézerat, J. Guyader, Force analysis technique: reconstruction of force distribution on plates, Acta Acust. 86 (2) (2000) 322–332.

[17] M. Djamaa, N. Ouelaa, C. Pézerat, J. Guyader, Reconstruction of a distributed force applied on a thin cylindrical shell by an inverse method and spatial filtering, Journal of Sound and Vibration 301 (3) (2007) 560 – 575. doi:https://doi.org/10.1016/j.jsv.2006.10.021.
URL http://www.sciencedirect.com/science/article/pii/S0022460X06007991

[18] T. Wassereau, Caractérisation de matériaux composites par problème inverse vibratoire (characterization of composite materials by inverse vibration problem), Ph.D. thesis, Université du Maine (Oct. 2016).

[19] H. Xu, L. Cheng, Z. Su, J.-L. Guyader, Identification of structural damage based on locally perturbed dynamic equilibrium with an application to beam component, Journal of Sound and Vibration 330 (24) (2011) 5963–5981. doi:https://doi.org/10.1016/j.jsv.2011.07.028.

[20] H. Xu, L. Cheng, Z. Su, J.-L. Guyader, Damage visualization based on local dynamic perturbation: Theory and application to characterization of multi-damage in a plane structure, Journal of Sound and Vibration 332 (14) (2013) 3438–3462. doi:https://doi.org/10.1016/j.jsv.2013.01.033.

[21] C. Renzi, C. Pézerat, J.-L. Guyader, Vibratory source identification by using the finite element model of a subdomain of a flexural beam, Journal of Sound and Vibration 332 (3) (2013) 545–562. doi:http://dx.doi.org/10.1016/j.jsv.2012.09.003.

[22] C. Renzi, C. Pézerat, J.-L. Guyader, Local force identification on flexural plates using reduced finite element models, Computers and Structures 144 (2014) 75–91. doi:http://dx.doi.org/10.1016/j.compstruc.2014.07.003.

[23] C. Renzi, Identification expérimentale de sources vibratoires par résolution du probléme inverse modélisé par un opérateur éléments finis local (experimental identification of vibration sources by solving of inverse problem modeled by a local finite operator), Ph.D. thesis, INSA de Lyon (Dec. 2011).
URL https://tel.archives-ouvertes.fr/tel-00715820

[24] K. Ege, N. Roozen, Q. Leclère, R. G. Rinaldi, Assessment of the apparent bending stiffness and damping of multilayer plates; modelling and experiment, Journal of Sound and Vibration 426 (2018) 129 – 149. doi:https://doi.org/10.1016/j.jsv.2018.04.013.
URL http://www.sciencedirect.com/science/article/pii/S0022460X18302384

[25] F. Ablitzer, C. Pézerat, J.-M. Génevaux, J. Bégué, Identification of stiffness and damping properties of plates by using the local equation of motion, Journal of Sound and Vibration 333 (9) (2014) 2454 – 2468. doi:http://dx.doi.org/10.1016/j.jsv.2013.12.013.
URL http://www.sciencedirect.com/science/article/pii/S0022460X13010535

[26] P. Bottois, N. Joly, C. Pézerat, F. Ablitzer, Identification of local young's modulus and loss factor of curved beam by using an inverse method and a finite element operator, INTER-NOISE and NOISE-CON Congress and Conference Proceedings 255 (5) (2017) 2165–2174.

[27] C. Faure, Approches bayésiennes appliqués à l'identification d'efforts vibratoire par la méthode de résolution inverse (bayesian approaches applied to the identification of vibratory forces by the inverse resolution method), Ph.D. thesis, Le Mans Université (2017).

[28] M. Géradin, D. Rixen, Mechanical Vibrations: Theory and Application to Structural Dynamics, 2nd Edition, MASSON, 1996.

[29] A. Leung, An accurate method of dynamic condensation in structural analysis, International Journal for Numerical Methods in Engineering 12 (1978) 1705 – 1715.

[30] K. Petersen, M. Pedersen, The matrix cookbook, 2012.
URL https://www.math.uwaterloo.ca/~hwolkowi/matrixcookbook.pdf

[31] C. Faure, F. Ablitzer, J. Antoni, C. Pézerat, Empirical and fully bayesian approaches for the identification of vibration sources from transverse displacement measurements, Mechanical Systems and Signal Processing 94 (Supplement C) (2017) 180 – 201. doi:https://doi.org/10.1016/j.ymssp.2017.02.023.
URL http://www.sciencedirect.com/science/article/pii/S0888327017300961

[32] T. Wassereau, F. Ablitzer, C. Pézerat, J.-L. Guyader, Experimental identification of flexural and shear complex moduli by inverting the timoshenko beam problem, Journal of Sound and Vibration 399 (2017) 86 – 103. doi:https://doi.org/10.1016/j.jsv.2017.03.017.
URL http://www.sciencedirect.com/science/article/pii/S0022460X17302560

[33] E. Manconi, B. R. Mace, Estimation of the loss factor of viscoelastic laminated panels from finite element analysis, Journal of Sound and Vibration 329 (19) (2010) 3928 – 3939. doi:https://doi.org/10.1016/j.jsv.2010.04.014.
URL http://www.sciencedirect.com/science/article/pii/S0022460X1000266X

[34] M. Ruzek, Experimental identification of the equation of motion in vibroacoustics, Theses, INSA de Lyon (Dec. 2013).
URL https://tel.archives-ouvertes.fr/tel-01149070

[35] M. Ruzek, J.-L. Guyader, C. Pézerat, Information criteria and selection of vibration models, The Journal of the Acoustical Society of America 136 (6) (2014) 3040–3050. arXiv:https://doi.org/10.1121/1.4900562, doi:10.1121/1.4900562.
URL https://doi.org/10.1121/1.4900562